UCLA
UCLA Electronic Theses and Dissertations

Title
The Effect of Side Chains of Polymer Donors on the Performance of Organic Photovoltaics

Permalink
https://escholarship.org/uc/item/31p074n0

Author
Wang, Chaochen

Publication Date
2018

Peer reviewed|Thesis/dissertation

eScholarship.org Powered by the California Digital Library
University of California

UNIVERSITY OF CALIFORNIA

Los Angeles

The Effect of Side Chains of Polymer Donors on the Performance of Organic Photovoltaics

A thesis submitted in partial satisfaction

of the requirements for the degree Master of Science

in Materials Science and Engineering

by

Chaochen Wang

2018

© Copyright by

Chaochen Wang
2018

ABSTRACT OF THE THESIS

The Effect of Side Chains of Polymer Donors on the Performance of Organic Photovoltaics

by

Chaochen Wang

Master of Science in Materials Science and Engineering

University of California, Los Angeles, 2018

Professor Yang Yang, Chair

Converting solar energy into electricity provides an effective solution to the energy crisis the world is facing today. Organic Photovoltaics have shown potential to harness solar energy in a cost-effective way. Extensive progress has been achieved in understanding OPV photophysical phenomena and in identifying key factors needed to improve organic solar cell device power conversion efficiency (PCE). The newly synthesized polymer BDTP-Bz-1 and BDTP-Bz-2 composed of alternating benzotriazole and phenyl substituted benzodithiophene (Figure 1), yield ≈ 8% PCEs when blended in a bulk-hetero-junction (BHJ) structure with electron acceptor materials such as ITCC. The donor polymer BDTP-Bz-2 showed better device performance including short circuit current density (J_{sc}), open circuit voltage (V_{oc}), and External Quentum Efficiency (EQE), which can contribute to its preference for the "face-on" polymer backbone orientation in which the π-conjugated polymer backbone planes lie parallel to the substrate

surface, resulting in maximal contacts between organic photoactive materials and the ITO anode coated with electron transport layer (ZnO). This orientation of the π-π stacked structures would favor charge transport across the interface. By AFM analysis, it was revealed that the BDTP-Bz-2 : ITCC active layer showed lower surface roughness (10.6 nm) than BDTP-Bz-1 : ITCC active layer (12.5 nm). Lower surface roughness also helped form better interface contact between the active layer and the electrode.

The thesis of Chaochen Wang is approved.

Ximin He

Ali Mosleh

Yang Yang, Committee Chair

University of California, Los Angeles

2018

Table of Contents

ABSTRACT OF THE THESIS ii

The thesis of Chaochen Wang is approved iv

Table of Contents v

List of Figures vii

List of Tables ix

List of Abbreviations x

Acknowledgments xii

1. Introduction 1

    1.1 Motivation 1

    1.2 Objective 1

2. Background 3

    2.1 Organic Photovoltaics Principles 3

3. Experimental Methods 20

    3.1 Synthesis route of BDTP-Bz-1 and BDTP-Bz-2 20

    3.2 Preparation of a ZnO Electron Transport Layer 25

    3.3 Fabrication of inverted solar cells 26

    3.4 Film and Device Characterization 28

4. Results and Discussion 30

    4.1 Device Structure 30

4.2 Polymer Donor Side Chain Dependency of OPV Device Performance..... 30

4.3 Surface Morphology of BDTP-Bz-1 and BDTP-Bz-2.....32

4.4 Proposed Mechanism..... 35

5. Conclusions.....38

6. Scope of Future Work.....39

7. References.....40

List of Figures

Figure 1.1: The Chemical Structure of BDTP-Bz-1 and BDTP-Bz-2.....2

Figure 2.1: Various types of solar cell energy efficiency conversion trend].....4

Figure 2.2: The Operating Principle of OPV.....5

Figure 2.3: Equivalent Circuit Diagram of Organic Solar Cell].....7

Figure 2.4: J-V Curve of Organic Solar Cel.....8

Figure 2.5: Organic solar cell device structure: a) single-layer structure; b) double heterojunction structure; c) bulk heterojunction structure; d) tandem structure.....13

Figure 2.6: Donor material molecular structures.....14

Figure 2.7: Acceptor material molecular structures.....15

Figure 3.1: Structure of PTB polymers represented by a segment representing the possible zig-zag or arched conformation the polymer backbone.....20

Figure 3.2: Structure of PTB polymers represented by a segment representing the possible zig-zag or arched conformation the polymer backbone.....36

Figure 3.3: 1H NMR of 4,8-bis(4-(2-ethylhexyl)phenyl)benzo[1,2-b:4,5-b']dithiophene (2)..... 37

Figure 3.4: 1H NMR of (4,8-bis(4-(2-ethylhexyl)phenyl)benzo[1,2-b:4,5-b']dithiophene-2,6-diyl)- bis(trimethylstannane) (M2).....37

Figure 3.5: 1H NMR of (4,8-bis(3,4-dibutylphenyl)benzo[1,2-b:4,5-b']dithiophene-2,6-diyl)-bis(trimethylstannane) (M3).....38

Figure 4.1: The basic structure of interted single - junction solar cell.....43

Figure 4.2: Current-voltage (J-V) curve of BDTP-Bz-1 and BDTP-Bz-2.....44

Figure 4.3: External Quantum Efficiency (EQE) of BDTP-Bz-1 and BDTP-Bz-2.....45

Figure 4.4: (a), (b) AFM image of BDTP-Bz-1 active layer; (c), (d) AFM image of BDTP-Bz-2 active layer.....46

Figure 4.5: Absorbance of film formed by BDTP-Bz-1 and BDTP-Bz-2.....48

List of Tables

Table 3.1: Composition of electron transport layer (ZnO) precursor solution..... 21

Table 4.1: Electrical properties of OPV with BDTP-Bz-1 : ITCC and BDTP-Bz-2 : ITCC as activce layers..... 32

List of Abbreviations

OPV	Organic Photovoltaics
PCE	Power Conversion Efficiency
AFM	Atomic Force Microscope
XRD	X-ray Diffraction
BHJ	Bulk-Hetero-Junction
CuPc	Copper Phthalocyanine
PDI	Perylenediimide
a-Si	Amorphous Si
HOMO	Highest Occupied Molecular Orbital
LUMO	Lowest Unoccupied Molecular Orbital
V_{OC}	Open Circuit Voltage
J_{SC}	Short Circuit Current Density
EQE	External Quantum Efficiency
FF	Fill Factor
GIWAXS	Grazing Incident Wide-Angle X-ray Scattering
R_S	Series Resistance
R_{SH}	Shunt Resistance
MIM	Metal/Insulator/Metal
IPA	Isopropanol

ITO	Indium-Tin Oxide
BDT	benzodithiophene
P3HT	Poly-3-hexylthiophene
TT	Thienothiophene
NDI	Naphthalimide
CF	Chloroform

Acknowledgments

I would like to convey my gratefulness to my supervisor, Prof. Yang Yang for his guidance and support during my graduate education. This work wouldn't have been possible without him.

I would like to thank Dr. Pei Cheng, Dr Jun Yuan and Dr. Chang Sung Yung for their guidance and support during this project, and for training me on various instruments and skills to carry out this research and these training will remain useful even after my graduation. Many thanks to Dr. Jun Yuan for the synthesis route for the materials, Dr. Zhengxu Wang for XRD, Dr. ShengYung Chang for AFM, Dr. Yuqiang Liu for Absorption. Also thank my fellow lab mates Rui Wang, Tianyi Huang, Haowen Zheng for designing and discussing our research together and it is very lucky to have you in OPV group.

I thank all the good people in YY lab. It is an unforgettable memory to work with the smartest people.

1. Introduction

1.1 Motivation

Since their discovery, organic conducting polymers have been intensely explored for a variety of potential optoelectronic applications.[1] Recently, organic photovoltaic (OPV) devices based on semiconducting polymers have emerged as attractive alternatives to inorganic solar cells due to their potential low manufacturing cost and processing flexibility. Extensive progress have been achieved in understanding OPV photophysical phenomena and in identifying key factors needed to improve organic solar cell device power conversion efficiency (PCE). The newly synthesized polymer BDTP-Bz-1 and BDTP-Bz-2 composed of alternating benzotriazole and phenyl substituted benzodithiophene (Figure 1), yield ≈ 8% PCEs when blended in a bulk-hetero-junction (BHJ) structure with electron acceptor materials such as ITCC (3,9-bis(4-(1,1-dicyanomethylene)-3-methylene-2-oxo-cyclopenta[b]thiophen)-5,5,11,11-tetrakis(4-hexylphenyl)-dithieno[2,3-d':2,3-d']-s-indaceno[1,2-b:5,6-b']-dithiophene). The structural defferences within these two polymers arise from the alkyl chains appended at different backbone positions, and also different side chain lengths, as shown in figure.

1.2 Objective

The aim of this work is to understand the effect of side chain of the polymer donor on device performance and based on this knowledge to study how the morphology of the active layer may affect the device performance.

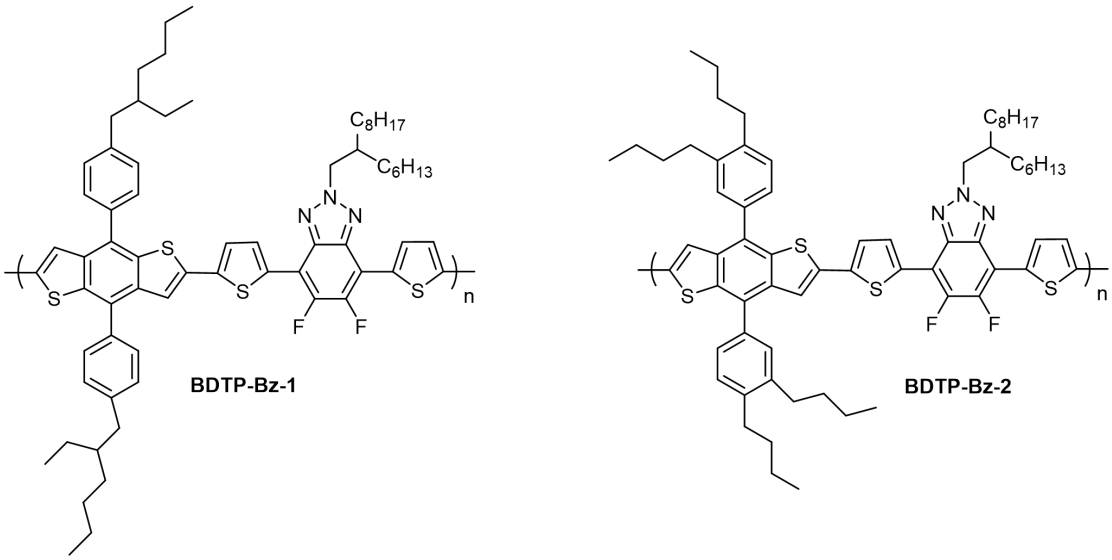

Figure 1. The Chemical Structure of BDTP-Bz-1 and BDTP-Bz-2

2. Background

2.1 Organic Photovoltaics Principles

As early as 1954, Bell Labs successfully prepared the first solar cell.[4] The first-generation solar cells are mainly based on single-crystal silicon and gallium arsenide, and the technology is now mature. The energy conversion efficiency is high, but due to its high cost, it is currently used in high-tech fields such as aerospace or defense. In order to achieve the goal of large-scale use of solar cells, reducing the cost of materials has become the main means of lowering the cost of solar power. Based on this idea, the second generation of solar cells uses thin film technology. The materials mainly include polysilicon, amorphous silicon, cadmium selenide and copper indium selenide. Unlike the second generation, the third generation of solar cell is based on the goal of improving the power conversion efficiency on a low-cost basis. Currently, it mainly includes dye-sensitized solar cells, organic solar cells, perovskite solar cells, quantum dot solar cells, and so on. (The development trend of the energy conversion efficiency of various types of solar cells is shown in Figure 2.1).

The research of organic solar cells can be traced back to 1959, when a single crystal of germanium was used as the active layer, the open-circuit voltage was only 200 mV, and the energy conversion efficiency was very low. In 1986, organic solar cells made a revolutionary breakthrough. Dr. Deng Qingyun of Kodak Company reported that copper phthalocyanine (CuPc) was used as a p-type semiconductor, and a perylenediimide (PDI) derivative was used as a pair of n-type semiconductors. Layers of organic solar cells have an energy conversion efficiency of about 1%. [5]

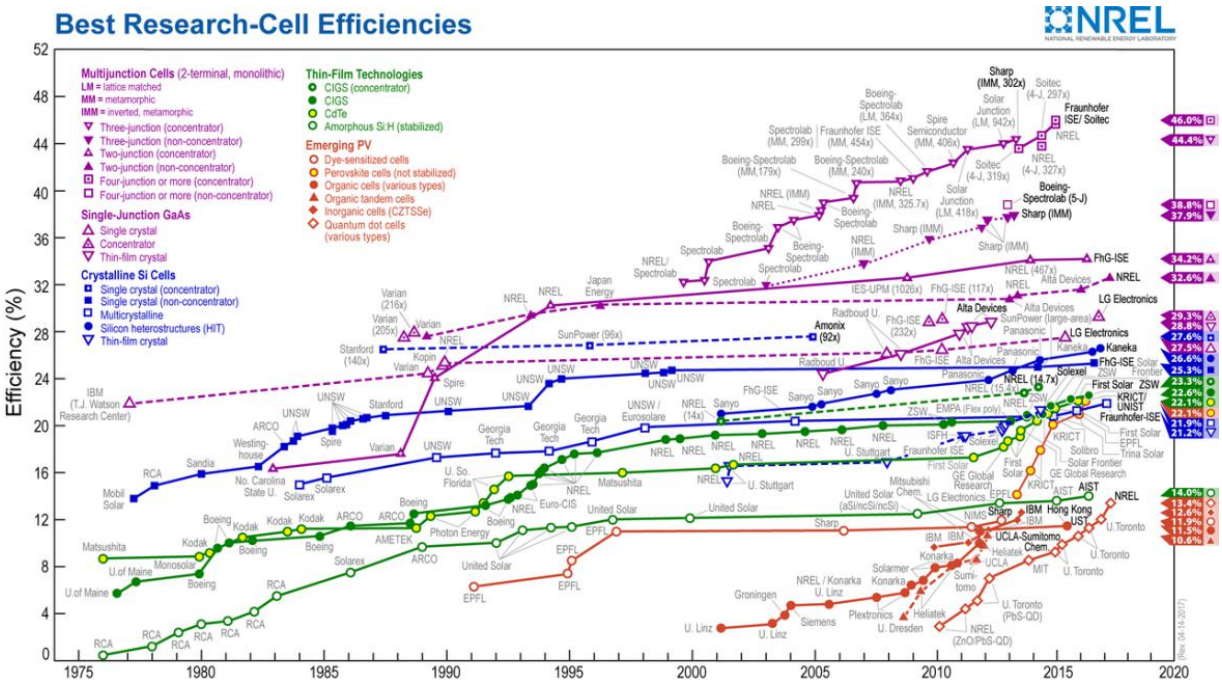

Figure 2.1 Various types of solar cell energy efficiency conversion trend

In 1992, Sariciftci et al. found that using conjugated polymers as donor materials and C_{60} as the acceptor material could induce rapid exciton dissociation under light induction, and the process was much faster than its inverse process. In 1995, Heeger et al. produced bulk heterojunction (BHJ) organic solar cells using donor-acceptor material blends for the first time, of which the conjugated polymer MEH-PPV was used as electron donor material and the solution-processable fullerene derivative PCBM was used as electron acceptor material for the first time. Due to the formation of an interpenetrating network between the donor and the acceptor material of this kind of bulk heterojunction organic solar cell, it can greatly increase the interface area and shorten the exciton diffusion distance, thereby significantly improving the energy conversion efficiency of the device.[7] In recent years, by synthesizing new acceptor materials, optimizing the active layer morphology, and introducing new device structures, the energy conversion efficiency of organic solar cells has exceeded 11%.

Basic principles of organic solar cells

Photovoltaic effect refers to: When irradiating a semiconductor with the light of the appropriate wavelength, due to light excitation and the building of electric field within the semiconductor, the potential will be generated. Photovoltaic effect is the theoretical basis for organic solar cells to realize photoelectric energy conversion. As shown in Fig. 2.2, the photoelectric conversion process of [11] organic solar cells mainly includes the following four steps: 1 Absorption of incident light to generate excitons; 2 Exciton diffusion; 3 Exciton dissociation; 4 Carrier transport and collection.

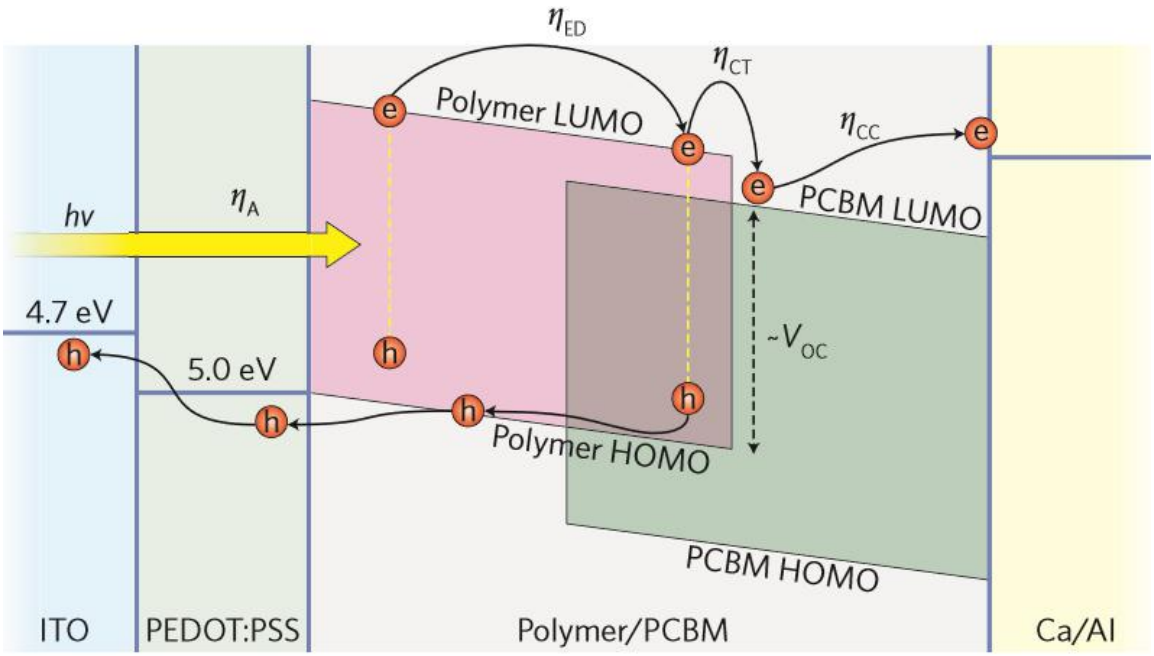

Figure 2.2. The Operating Principle of OPV

1.Absorption of incident light to generate excitons

After an organic semiconductor material absorbs a photon with a certain energy, it excites an electron to jump from its highest occupied molecular orbital (HOMO) to its lowest unoccupied molecular orbital (LUMO) while leaving a vacancy at the HOMO. This vacancy is called a hole.

With positive charge. This electron-hole pair (exciton) is bound together by the Coulomb force of positive and negative charges (usually has strong binding energy).

2..Exciton diffusion

The excitons generated after the photoactive layer absorbs photons need to diffuse to the interface of the acceptor to undergo the next exciton dissociation. In general, the exciton diffusion distance in the conjugated polymer is less than 10 nm, and photoexcites other than 10 nm from the donor interface are difficult to transmit to the donor/acceptor interface and do not contribute to the photoelectric conversion. In addition, if the exciton recombines during the diffusion process, it also does not contribute to the photoelectric conversion.

3. Exciton dissociation

The exciton diffuses to the donor/acceptor interface, where the electrons are transferred to the LUMO level of the acceptor material, and the vacancy remains at the HOMO level of the donor material, thereby exciton dissociation. The dissociated excitons become independent electrons and holes.

4.Carrier transport and collection

Under the effect of the electric field inside the organic solar cell, the dissociated holes are formed along the donor material. The channel is transported to the anode, and electrons are transported to the cathode along the channel formed by the acceptor material. Electrons and holes. After being collected by the cathode and the anode, respectively, an anode-to-cathode photocurrent can be formed in the external circuit, thereby generating a photovoltaic effect.

Organic solar cell performance parameters

The organic solar cell can be equivalent to the following circuit diagram (Fig. 2.3). 14 is composed of a diode, a current source, a voltage source, and a resistor.

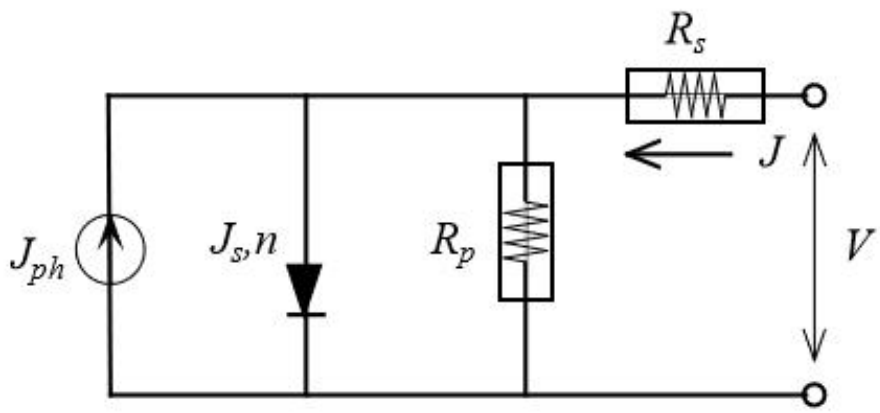

Figure 2.3 Equivalent Circuit Diagram of Organic Solar Cell

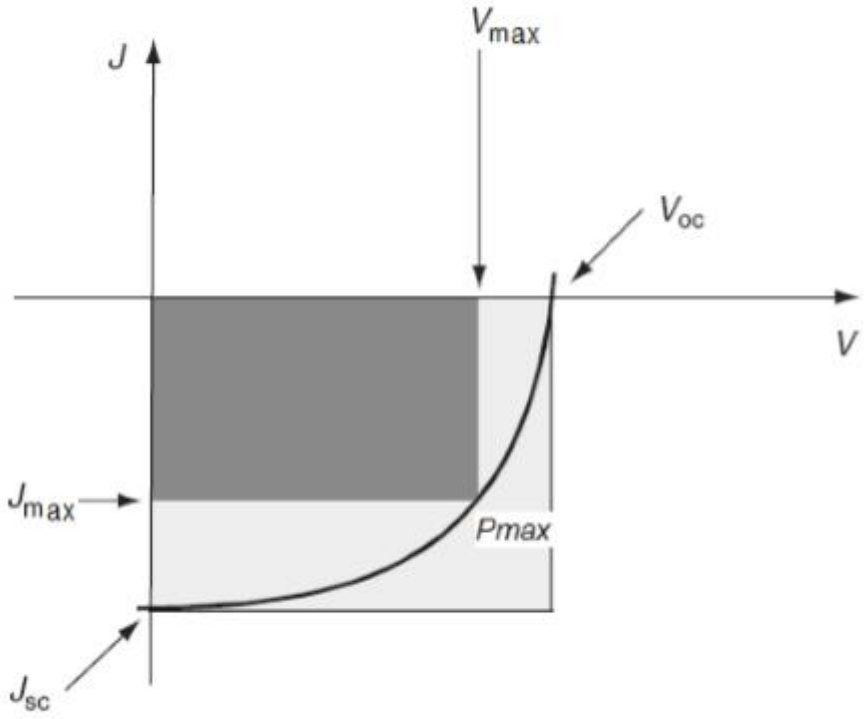

Figure 2.4 J-V Curve of Organic Solar Cell

1. Open circuit voltage (V_{OC})

The maximum output voltage of an organic solar cell is the voltage at which the positive and negative electrodes of the solar cell are opened under illumination, and the unit is volts (V). The carriers at the photocell heterojunction all accumulate near the junction and maximize the original contact potential barrier, resulting in the largest photocurrent electromotive force. For single-layer solar cells, the VOC is determined by the difference in the work function of its positive and negative electrodes; [15] for the donor-acceptor blending heterojunction solar cells, Voc usually have a positive correlation with the energy level difference between the HOMO of the donor material and the LUMO of the acceptor material. [16]

2. Short-circuit current density (J_{SC})

The maximum output current density of an organic solar cell refers to the current density when the positive and negative electrodes of the organic solar cell are short-circuited in the light, and the unit is mA cm^{-2}. When short-circuited, at the interface to the acceptor material, the separated carriers will not accumulate at the interface with the acceptor material and will all flow through the external circuit, producing a maximum value of photocurrent density.

3. Fill factor (FF)

The fill factor indicates the ability of the organic solar cell to provide the maximum output power externally. At the same time it also represents the ability of organic solar cells to prevent energy loss, that is, the greater the FF value, the smaller the energy loss. In simple terms, FF is the ratio of the shaded area of the rectangle (Pmax = Vmax × Jmax) and the area of the dashed rectangle ($V_{OC} \times J_{SC}$).

$$FF = \frac{p_{\max}}{V_{oc} J_{sc}} = \frac{J_m V_m}{V_{oc} J_{sc}}$$

4. Power Conversion Efficiency (η or PCE)

The energy conversion efficiency is the percentage of the amount of energy that indicates how much of the incoming sunlight's energy translates into effective energy.

defined as:

$$\eta = \frac{P_{\max}}{V_{oc} J_{sc}} \times 100\% = \frac{J_{\max} V_{\max}}{P_{in}} \times 100\% = \frac{J_{sc} V_{oc} FF}{P_{in}} \times 100\%$$

5. External quantum efficiency (EQE)

The proportion of electrons generated by each incident photon at a given wavelength that can be sent to an external circuit, is defined as:

$$EQE = \frac{1240 \times J_{sc}}{\lambda \times P_{in}}$$

Where λ is the wavelength of the incident light, Pin is the power of the incident light, and J_{SC} is the short-circuit current density.

6. Series Resistance (R_S)

In the equivalent circuit diagram (Figure 2.3), the series resistance is equivalent to the impediment of carriers traveling in the vertical direction. When the voltage is close to the open-circuit voltage V_{OC}, the J-V curve is close to the linear curve, and the series resistance R_S can be calculated from the reciprocal of its slope:

$$R_s \approx (\frac{I}{V})^{-1}$$

7. Shunt Resistance (R_{SH})

In the equivalent circuit diagram (Figure 2.3), the parallel resistance is equivalent to the resistance of the organic solar cell itself (ie load).When the voltage is close to 0 V, the J-V curve is close to the linear curve, then the parallel resistance RSH can be calculated from the reciprocal of its slope:

$$R_p \approx (\frac{I}{V})^{-1}$$

Organic solar cell basic structure

1. Single-layer structure

Single-layer organic solar cells are shown in Figure 2.5a. The polymer is sandwiched between two electrodes with different work functions. [17] This type of structure is also referred to a metal/insulator/metal (MIM) structure. Due to the dielectric constant the of polymer material

is very low, and it is difficult to effectively dissociate the excitons by simply relying on the work function difference between the two electrodes, in a single layer, the exciton is easily recombined back to the ground state, so the power conversion efficiency of this single-layer device is usually very low.[16]

2. Double heterojunction structure

To overcome the problem of exciton dissociation in single-layer organic solar cells, the acceptor materials were placed in two layers of the device to increase the exciton dissociation efficiency of the photoactive material (Figure 2.5b). The double-layered device based on small molecule materials and polymer materials was first time reported by Deng Qingyun [5] and Sariciftci et al. in 1986 and 1993 respectively. In this device structure, the exciton is at the interface to the acceptor, driven by the difference in the energy levels of the acceptor materials, which can effectively overcome the larger binding energy and exciton dissociation. The advantage of this structure is that the exciton dissociation driving force is strong; The carrier transport channels are open, with few recombinations; Electrons and holes can be efficiently collected by the cathode and anode. Currently, a single-cell organic solar cell based on a double-layer structure can achieve a power conversion efficiency of up to 8.3%. [20] This structure also has its disadvantages: due to the exciton diffusion distance of organic material is generally only about 10 nm, a large number of

photogenerated excitons are captured during the transmission; at the same time, the dissociation of excitons is still insufficient because of the small interface to the acceptor material.

3. Bulk heterojunction structure

In 1995, Heeger et al. blended C_{60} with MEH-PPV to prepare the first bulk heterojunction organic solar cell (Figure 2.5c).[7] The formation of such a blended structure can greatly increase the interface area between the acceptor materials so that the exciton can be effectively dissociated. The bulk heterojunction structure is the most successful organic solar cell structure at present. After 20 years of development, the organic solar cell can obtain the energy conversion efficiency of up to 11.7% based on this structure.

4. Tandem structure

As shown in Figure 2.5d , the tandem structure is to connect single organic solar cells in parallel or in series. Paralleling can achieve large short-circuit current densities and series can achieve high open-circuit voltages. because the tandem structure can be better utilize solar energy (two single-cell batteries can absorb complementarily), the energy conversion efficiency of organic solar cells based on this structure has reached 11.8% in 2014.

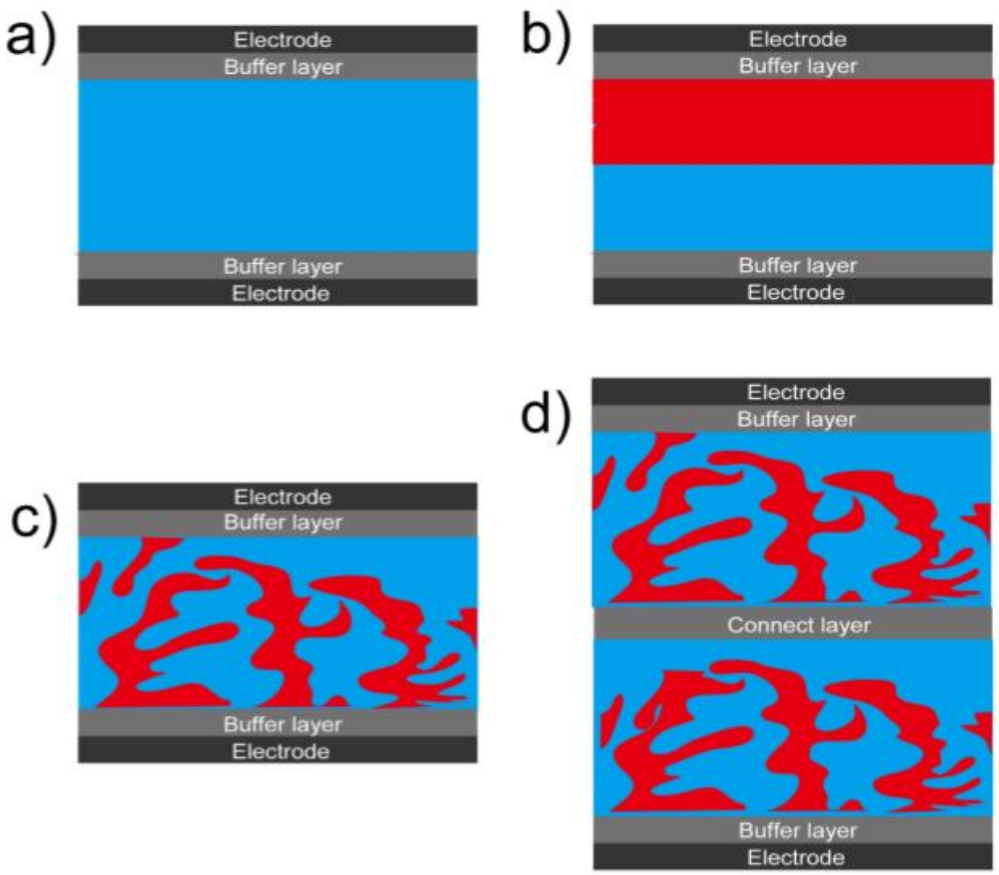

Figure 2.5 Organic solar cell device structure: a) single-layer structure; b) double heterojunction structure; c) bulk heterojunction structure; d) tandem structure.

Organic solar cell active layer material profile

The active layer of an organic solar cell consists of an electron donor material and an electron acceptor material. Electron donating materials (Figure 2.6) can be classified into polymer materials and small molecule materials, while electron acceptor materials (Figure 2.7) can be classified into fullerene materials and non-fullerene materials.

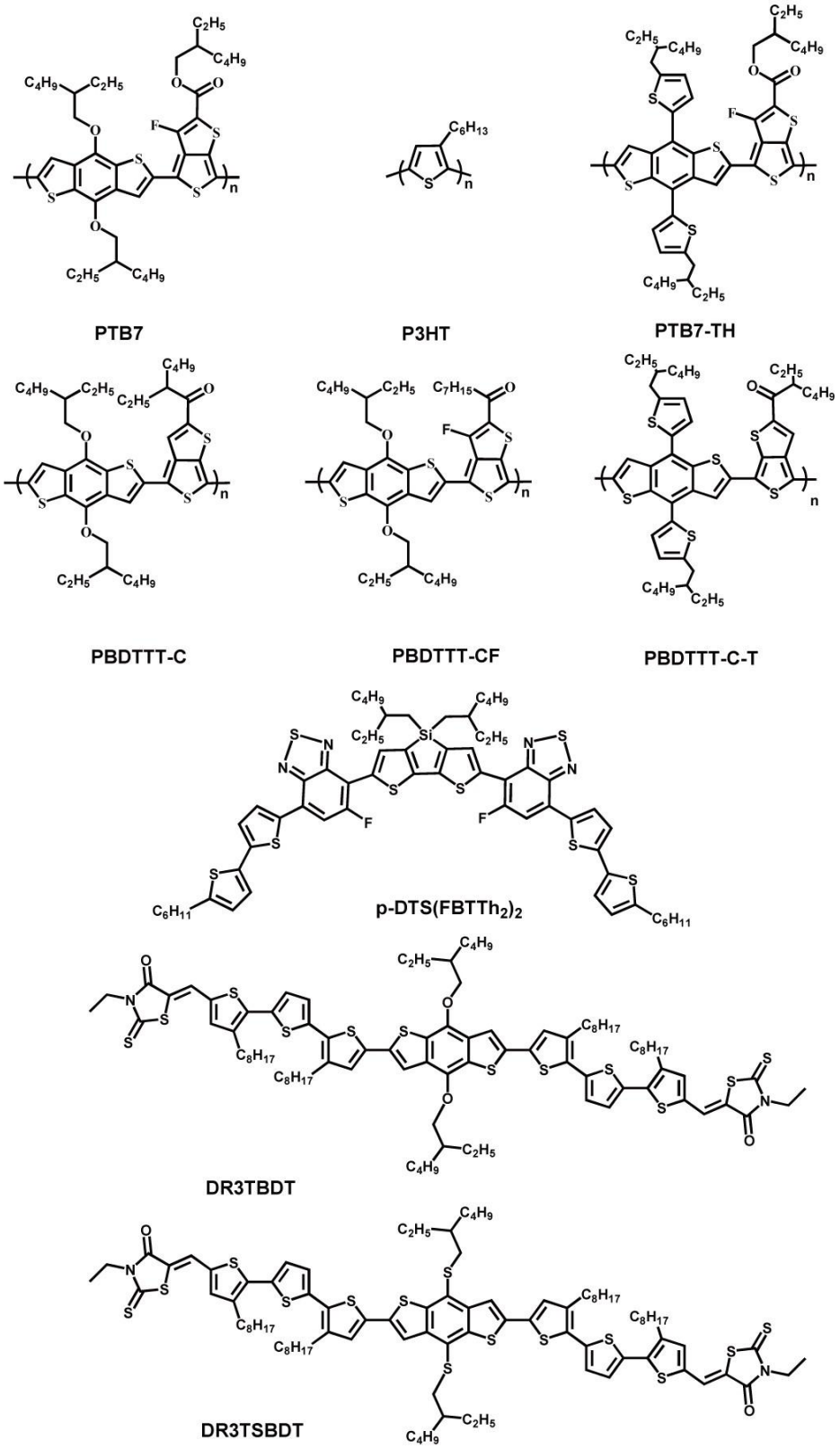

Figure 2.6 Donor material molecular structures

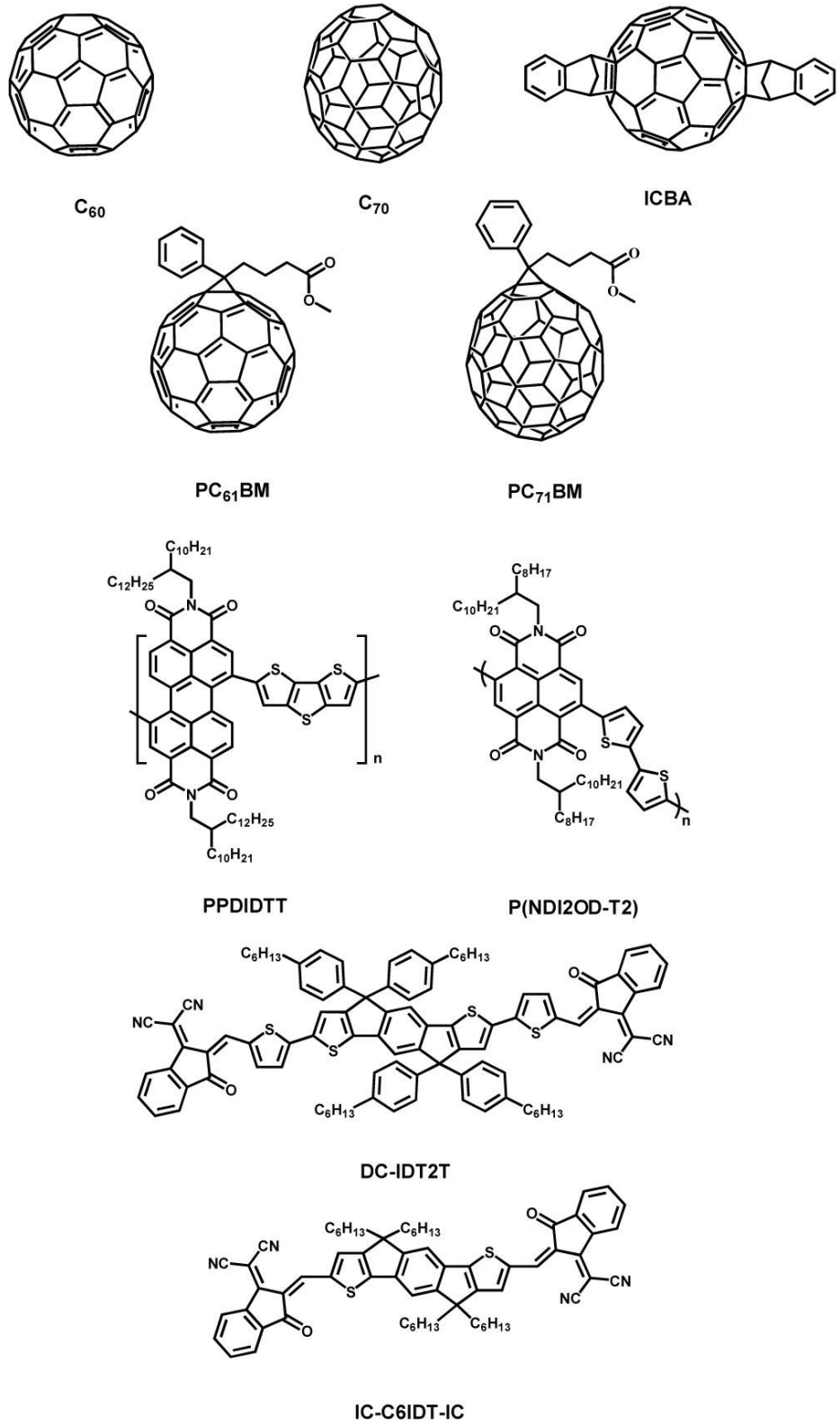

Figure 2.7 Acceptor material molecular structures

1. Polymer donor materials

Since 2002, poly-3-hexylthiophene (P3HT) has been favored by researchers because of its simple structure, low price, and high hole mobility. Based on P3HT/PC61BM, most of the research groups can produce organic solar cells with energy conversion efficiency of 3-4%.[24] for the sake of step by step optimization of polythiophene donor materials, the researchers also studied the molecular weight of the polymer, the degree of regional regularity and type of alkyl chain and device performance. However, P3HT also has serious drawbacks. Its absorption edge is only 650 nm, which greatly restricts its performance.

In recent years, a wide range of absorption (absorption edge 750-800 nm) and higher mobility have given rise to receptors polymers have received more attention from researchers. Of the large number of novel copolymers for receptor-copolymers, [25-30] based on benzodithiophene (BDT) units are among the most successful polymer donors. In 2009, Hou et al.[31] reported that BDT unit-based polymer donor PBDTTT-C, which was prepared by blending it with $PC_{71}BM$, had an energy conversion efficiency of 6.58%. Further, by introducing fluorine atoms (PBDTTT-CF) on PBDTTT-C, the HOMO energy level is significantly reduced, and the open circuit voltage of the organic solar cell can be increased. The energy conversion efficiency of the organic solar cell prepared by blending PBDTTT-CF with PC71BM was as high as 7.73% (validation value 6.77%), which was the highest efficiency reported at the time. In 2010, Yu et al34 reported on a polymer based on BDT unit PTB7, which has different alkyl side chains compared to PBDTTT-CF. After optimized device preparation conditions, the energy conversion efficiency of PTB7/$PC_{71}BM$-based organic solar cells reached 7.4%.

In 2011, Hou[33] et al. further optimized the BDT units of PBDTTT-C polymers. They replaced the original alkoxy groups (PBDTTT-C-T) with phenyl groups. Since the BDT unit was changed

from one-dimensional conjugation to two-dimensional conjugation, the short-circuit current density of PBDTTT-C-T/$PC_{71}BM$-based organic solar cells was further improved, and its energy conversion efficiency was as high as 7.59%. Based on this two-dimensional conjugate strategy, in 2013, Chen et al.[34] further optimized the BDT units of PTB7 polymers. They also replaced the original alkoxy groups (PTB7-TH) with phenyl groups. Under the same preparation conditions as the PTB7/$PC_{71}BM$ organic solar cell, the energy conversion efficiency of the PTB7-TH/$PC_{71}BM$-based organic solar cell reached 8.4%. In view of the excellent performance of the polymer donor containing BDT unit, the polymer donor chosen for this project is mainly (PBDTTT-C-T, PTB7, PTB7-TH) system.

2. Small molecule donor materials

In recent years, small-molecule donor materials have also been studied carefully due to their high purity and small batch differences. Similar to polymer materials, small-molecule donor materials with narrower band gaps and higher hole mobility typically also exhibit better performance. In 2012, Bazan et al.[38] reported on a small-bandwidth, small-molecule donor material, p-DTS $(FBTTh_2)_2$. The energy conversion efficiency of organic solar cells prepared by blending this material with $PC_{71}BM$ reached 7.0%. A small molecule organic solar cell has been reported with more than 7% energy conversion efficiency. In the same year, Chen et al.[39] reported on the small molecule donor material DR3TBDT based on BDT cells. The energy conversion efficiency of the organic solar cell prepared by blending this material with $PC_{71}BM$ was as high as 7.38%. In 2014, Chen et al.[40] further optimized the small molecule donor materials based on BDT units. They changed the alkoxy groups on the BDT units to alkylthio groups (DR3TSBDT). The small molecule organic solar cell prepared by blending DR3TSBDT with $PC_{71}BM$ has an energy conversion efficiency as high as 9.95%.

3. Fullerene acceptor materials

Fullerene is a spherical molecule. Because fullerenes have a strong ability to absorb electrons and ultrafast exciton dissociation is achieved at the body interface, and it and its derivatives are the main choices for acceptor materials for a long time. The earliest organic solar cells used were C_{60} and C_{70} fullerene molecules, which were used in vapor-deposited double-layer organic solar cells. However, due to the fact that fullerene balls contain only carbon, their solution processing performance has been greatly limited, so researchers have made various chemical modifications to fullerene to increase its solubility. Of the numerous fullerene derivatives, $PC_{61}BM$ and $PC_{71}BM$ are the most successful fullerene acceptor materials. Almost all organic solar cells with energy conversion efficiencies greater than 10% are based on PCBM. The LUMO level of PCBM is about -4.0 eV, and its lower LUMO level reduces the open-circuit voltage of organic solar cells. To overcome this shortcoming, the researchers increased the LUMO level of fullerenes by double addition reaction on fullerenes. Based on this strategy, the most successful molecule is ICBA. In 2010, Li et al. synthesized ICBA and blended it with P3HT to prepare an organic solar cell, resulting in an energy conversion efficiency of 5.44%.

4. Non-fullerene acceptor materials

Fullerene molecules also have some disadvantages, such as their weak absorption in the visible region, their almost no absorption in the near-infrared region, their high price, their tendency to dimerize under the influence of light, and their ability to crystallize easily when heated. In order to overcome these shortcomings, some novel receptor molecules (ie non-fullerene acceptor materials) have been synthesized and applied to organic solar cells. In 2007 and 2009, Zhan et al. and Facchetti et al. synthesized PDI and naphthalimide (NDI)-based polymer acceptor materials PPDIDTT and P(NDI2OD-T2), respectively.

However, due to the very severe PDI and NDI molecule aggregation and weak absorption in the near-infrared region, energy conversion efficiencies of non-fullerene organic solar cells based on PDI polymer and NDI polymer are relatively low for quite a long time. In 2015, Zhan et al. reported on the DC-IDT2T, an acceptor material based on the IDT cell. Compared with PDI polymers and NDI polymer materials, the greatest advantage of DC-IDT2T is its strong absorption in the near-infrared region and a greater contribution to photocurrent density. Non-fullerene organic solar cells based on this acceptor material and PBDTTT-CT polymer donor material have an energy conversion efficiency of 3.93%, which breaks the monopoly of non-fullerene acceptors based on PDI materials and NDI materials. . In 2016, Zhan et al. further optimized IDT-based receptor materials (IC-C6IDT-IC) through molecular design. The energy conversion efficiency of non-fullerene organic solar cells based on this acceptor material is as high as 8.71%.

3. Experimental Methods

Previous studies reported the synthesis of seven PTB polymers with the same alternating thienothiophene (TT) and benzodithiophene (BDT) backbone sequence but with varied side chains; their corresponding solar cell PCEs range from 2-8%. The structural difference among these seven polymers arise from the aliphatic side chains appended at different backbone positions, as shown in Figure 3.1. According to this knowledge, this essay studied the effect of different side chains of polymer donors on the performance of the device.

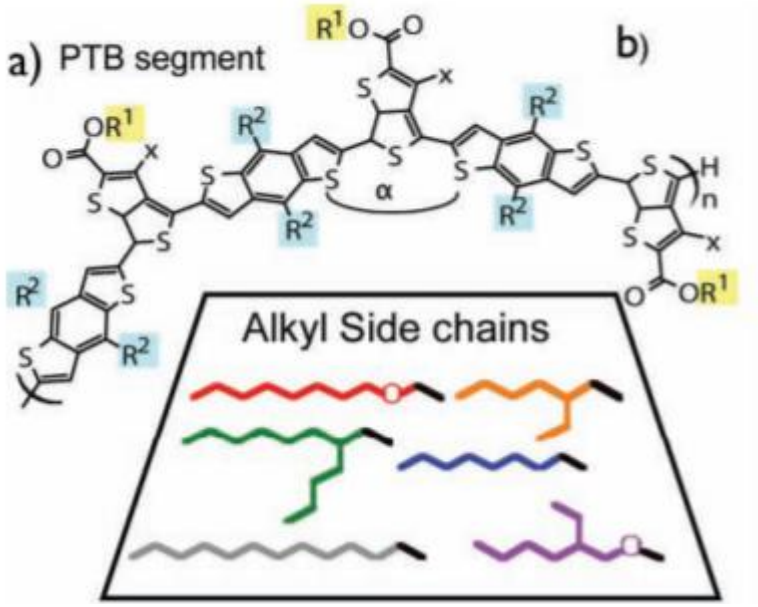

Figure 3.1 Structure of PTB polymers represented by a segment representing the possible zig-zag or arched conformation the polymer backbone.

3.1 Synthesis route of BDTP-Bz-1 and BDTP-Bz-2

4,8-bis(4-(2-ethylhexyl)phenyl)benzo[1,2-b:4,5-b']dithiophene (2)

Under vigorous stirring, 1-bromo-4-(2-ethylhexyl)benzene (8.04 g, 30 mmol) was added

dropwisely to magnesium turnings (0.86 g, 36 mmol) in anhydrous THF (50 mL) which was protected by argon. During the process, I2 (10 mg) was added as catalyst in the reaction. The solution was refluxed for 5h until the magnesium was consumed. The mixture was refluxed for one more hour and then was cooled down. The solution system was added slowly to benzo[1,2-b:4,5-b']dithiophene-4,8-dione (2.20 g, 10 mmol) dispersed in 40 mL THF. $SnCl_2$ (14.4 g) was dissolved in 10% aqueous HCl (20.2 mL) and then added dropwisely into the above reaction mixture. The solution was stirred for another 1 h at 50 °C. After cooling to room temperature, the mixture was poured into water and extracted with dichloromethane, the organic extraction was washed successively with water and sodium bicarbonate solution twice and the combined organic phase was dried over magnesium sulfate and evaporated to afford the crude product. The crude product was purified on a silica gel column, eluting with pure hexane. White crystals were obtained (2.3 g, 41% yield). 1H NMR (400 MHz, CDCl3) δ 7.61 (d, J = 8.1 Hz, 4H), 7.39 (d, J = 5.7 Hz, 2H), 7.34 (dd, J = 6.9, 2.4 Hz, 6H), 2.65 (d, J = 7.0 Hz, 4H), 1.72 – 1.63 (m, 2H), 1.43 – 1.26 (m, 16H), 0.98 – 0.86 (m, 12H).

(4,8-bis(4-(2-ethylhexyl)phenyl)benzo[1,2-b:4,5-b']dithiophene-2,6-diyl)bis(trimethylstannane) (M2)

A solution of compound 2 (1.0 g 1.8 mmol) in dry THF (30 mL) was deoxygenated with nitrogen for 30 min, and then 2.4 M n-butyllithium solution in n-hexane (1.9 mL, 4.50 mmol) was added dropwisely at 0 °C. Then the solution was allowed to warm up to 50 °C for 1 h, and 1.0 M trimethyltin chloride solution in THF (7.2 mL, 7.2 mmol) was added. Then the mixture was poured into water and extracted with dichloromethane. The organic phase was evaporated, and the residue was recrystallized from 20 mL acetone to afford the pale yellow solid (1.1 g, 68%). 1H NMR (400 MHz, $CDCl_3$) δ 7.63 (d, J = 8.1 Hz, 4H), 7.37 (t, J = 3.1 Hz, 4H), 7.34 (s,

2H), 2.66 (dt, J = 8.6, 4.4 Hz, 4H), 1.74 – 1.67 (m, 2H), 1.44 – 1.30 (m, 16H), 0.98 – 0.89 (m, 12H), 0.43 – 0.27 (m, 18H).

(4,8-bis(3,4-dibutylphenyl)benzo[1,2-b:4,5-b']dithiophene-2,6-diyl)bis(trimethylstannane) (M3)

M3 was synthesized similarly as described above for M2 (1.2 g, 74 %). 1H NMR (400 MHz, CDCl3) δ 7.52 (dd, J = 5.9, 1.9 Hz, 4H), 7.41 (d, J = 15.3 Hz, 2H), 7.36 – 7.32 (m, 2H), 2.78 – 2.69 (m, 8H), 1.74 – 1.62 (m, 8H), 1.53 – 1.42 (m, 8H), 1.02 (t, J = 7.3 Hz, 6H), 0.97 (t, J = 7.3 Hz, 6H), 0.42 – 0.27 (m, 18H).

Synthesis of BDTP-Bz-1

M1 (0.140 g, 0.2 mmol), M2 (0.178 g, 0.2 mmol) and 12 mL of dry toluene were put into a two-necked flask. The solution was flushed with Ar for 20 min, then Pd(PPh3)4 (15 mg) was added into the flask. The solution was flushed with Ar again for 20 min. The oil bath was heated to 110 °C carefully, and the reactant was stirred for 24 h at this temperature under argon atmosphere. Then the reaction mixture was cooled to room temperature and then poured into methanol (100 mL) slowly. The resulting precipitate was filtered through a Soxhlet thimble, which was then subjected to Soxhlet extractions with methanol, hexane and chloroform. Finally the polymer was recovered as a solid from the chloroform fraction by rotary evaporation. Finally, the dark-red solid was obtained (0.166 g, yield: 75%).

Synthesis of BDTP-Bz-2

BDTP-Bz-2 was obtained by the similar procedure with the synthesis of BDTP-Bz-1 starting from M1 (0.140 g, 0.2 mmol) and M3 (0.178 g, 0.2 mmol). Finally, the dark-red solid was obtained (0.180 g, yield: 81%).

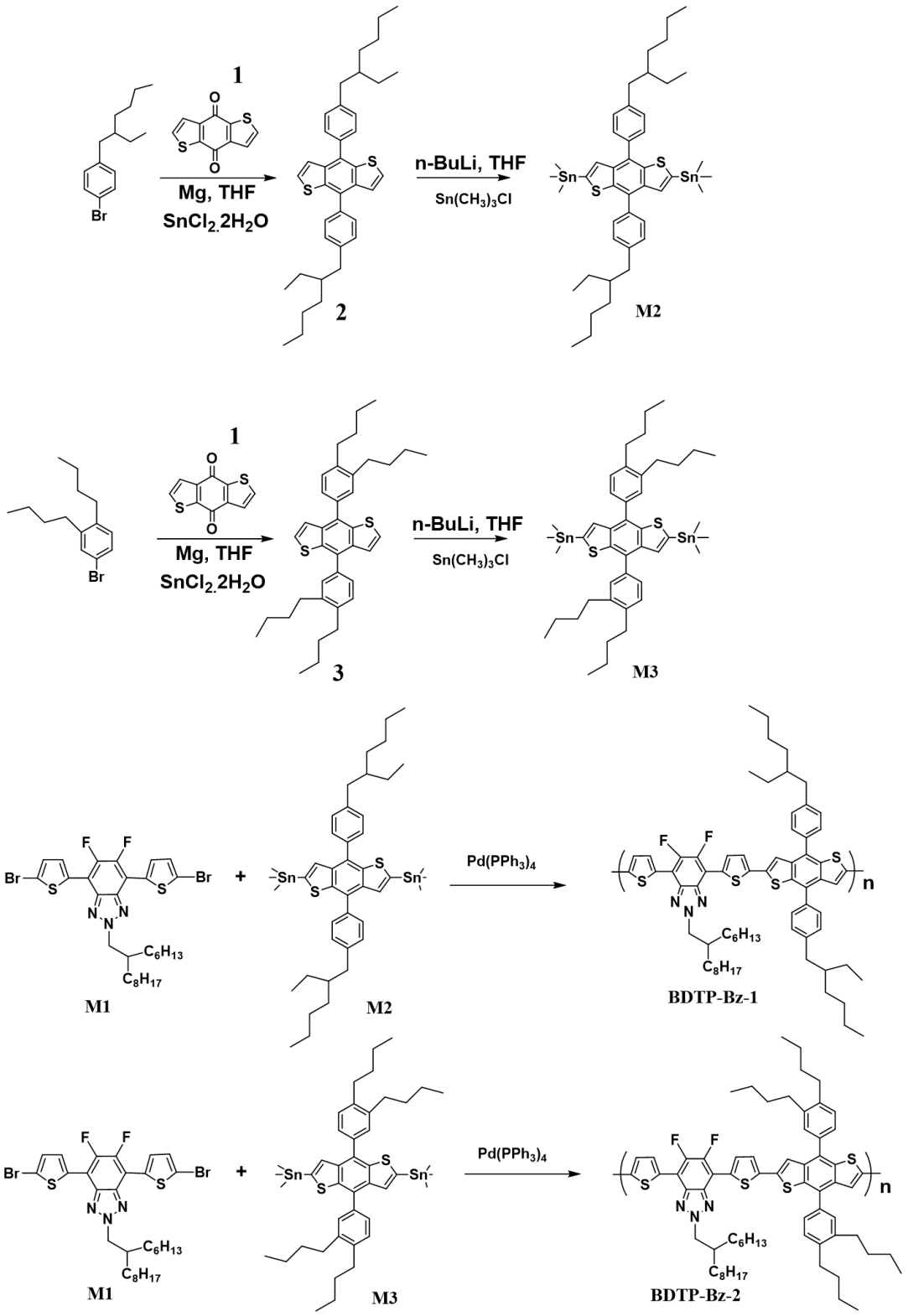

Figure 3.2 Structure of PTB polymers represented by a segment representing the possible zig-zag or arched conformation the polymer backbone.

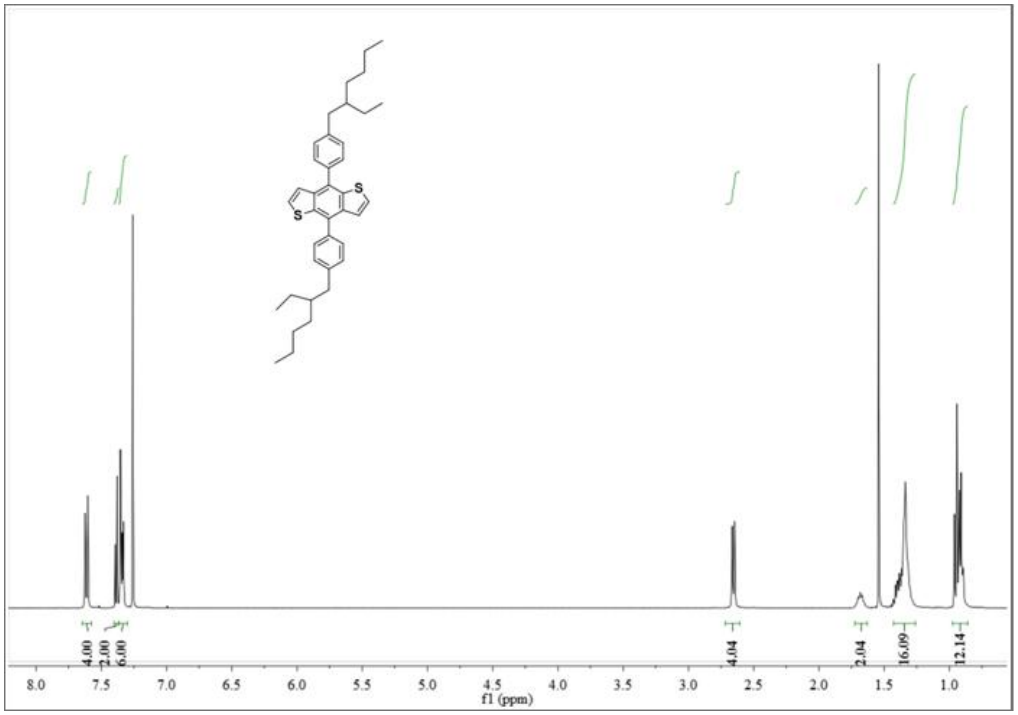

Figure 3.3. 1H NMR of 4,8-bis(4-(2-ethylhexyl)phenyl)benzo[1,2-b:4,5-b']dithiophene (2)

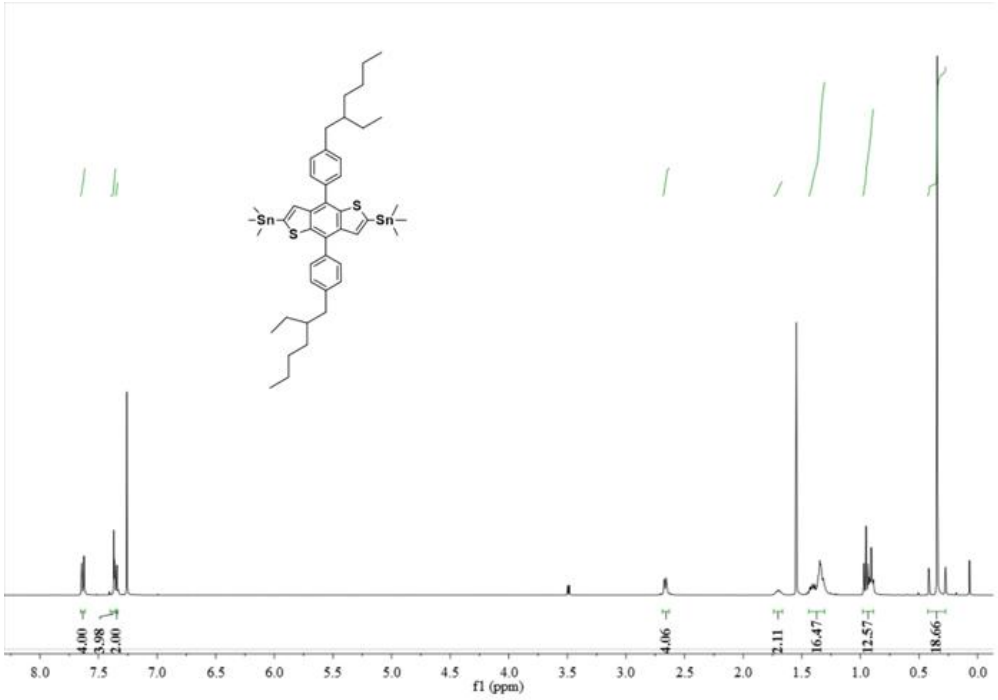

Figure 3.4 1H NMR of (4,8-bis(4-(2-ethylhexyl)phenyl)benzo[1,2-b:4,5-b']dithiophene-2,6-diyl)-bis(trimethylstannane) (M2)

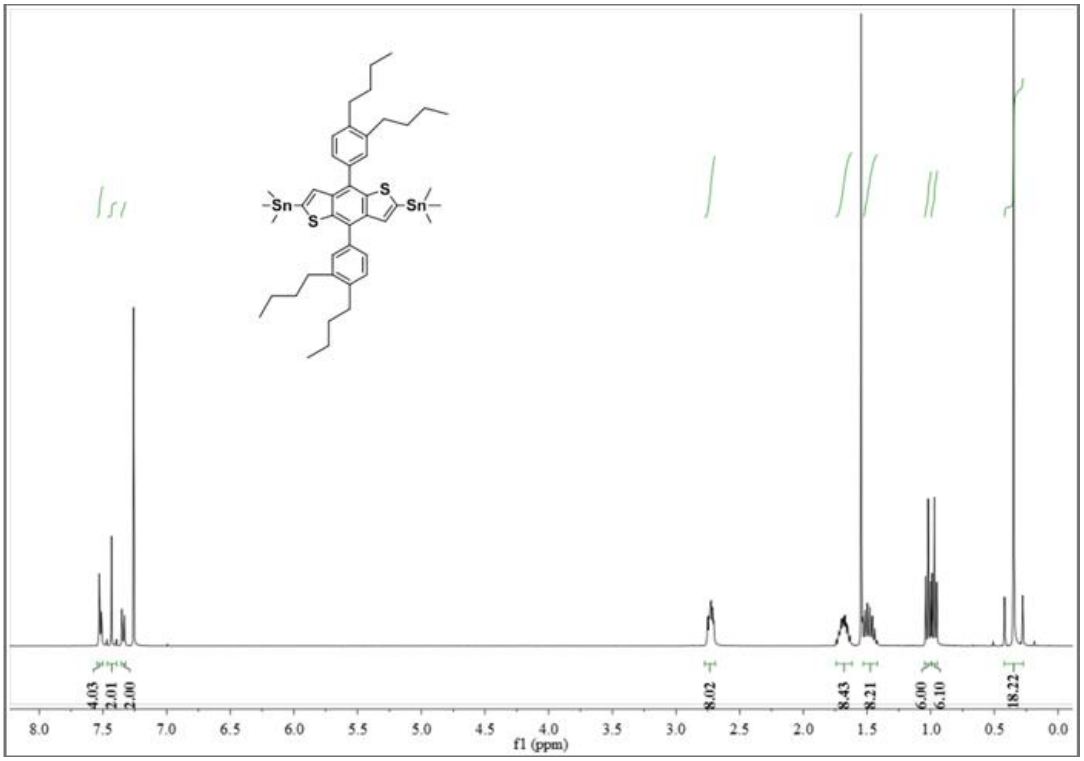

Figure 3.5 1H NMR of (4,8-bis(3,4-dibutylphenyl)benzo[1,2-b:4,5-b']dithiophene-2,6-diyl)-bis(trimethylstannane) (M3)

3.2 Preparation of a ZnO Electron Transport Layer

The zinc oxide precursor solution was prepared by dissolving equimolar ratios of zinc acetate dihydrate (ZAD) ($Zn(CH3COO)_2 \cdot 2H_2O$, Sigma Aldrich 99.9%) and monoethanol amine (MEA) ($NH_2CH_2CH_2OH$) in 2-methoxy ethanol (CH3OCH2CH2OH, Sigma Aldrich 99.8%) at room temperature (RT). The precursor solution was continuously stirred at RT for ~ 24 hours to induce hydrolysis in air. The freshly prepared ZnO precursor solution was spin-coated on cleaned, patterned ITO substrates (15 Ω sq^{-1}) for different spin rates varying from 1500–6000 rpm for 60 s. After the spin-casting process, the ZnO films were annealed in air on a hot plate (PRAZITHERM PZ 28-3TD) at 200 °C for 60 min and allowed to cool down at RT.

The zinc oxide nano particle solution was prepared by diluting zinc oxide solution (Sigma Aldrich 2.5%) to 2% with 2-propanol (IPA). The prepared zinc oxide solution was stirred at RT for 1 min to be completely mixed. The freshly prepared ZnO nanoparticle solution was spin-coated on cleaned, patterned ITO substrates (15 Ω sq−1) for different spin rates varying from 1500–6000 rpm for 60 s. After the spin-casting process, the ZnO films were annealed in air on a hot plate (PRAZITHERM PZ 28-3TD) at varying temperature from 60°C to 120°C for 60s and allowed to cool down at RT.

Table 3.1 Composition of electron transport layer (ZnO) precursor solution

Solution	Precursor	Additive
ZnO sol gel	ZAD	MEA
ZnO nano particle	None	None

3.3 Fabrication of inverted solar cells

Inverted solar cells were fabricated on pre-patterned ITO-coated glass. The ITO-coated glass substrates were subsequently cleaned with detergent (SDS), ultrasonicated in DI water, acetone, isopropyl alcohol and exposed to UV – ozone. The polymer blend solution was prepared by dissolving 6 mg of BDTP-Bz-1 (or BDTP-Bz-2) and 9 mg of ITCC in 1 mL of chloroform (CF). The solution was kept under stirring at 60 °C for ~ 30min before deposition. Approximately a 200 nm thick P3HT:PCBM based active layer is spun cast (1500 rpm, 60 s) on glass/ITO/ZnO substrates inside a N_2 filled glove box and the films were left in a glass Petri dish at RT for 24 h for slow solvent evaporation.

The photoactive polymer blend solution for the low bandgap material PTB7:$PC_{71}BM$ was prepared by mixing chlorobenzene of 1 : 1.5 w/w ratio (concentration of 25 mg mL−1) with 1,8-

diiodooctane (DIO) of 3% volume ratio and stirred overnight at 60 °C. An active layer with an approximate thickness of ~ 100 nm was obtained by spin casting the blend solution at 800 rpm for 60 s.

Later, the structure comprising glass ITO/ZnO/organic active layer was transferred to a vacuum thermal evaporator (5×10^{-6} bar base pressure) for MoO_3 (1.6 nm) and Ag (180 nm) thermal evaporation, using a shadow mask. The active area of the devices was 0.1 cm^2. For all the inverted device structures investigated in this study, all processing conditions related to the active layer spin-casting, to the top MoO_3 buffer layer deposition and Ag electrode deposition, were kept the same.

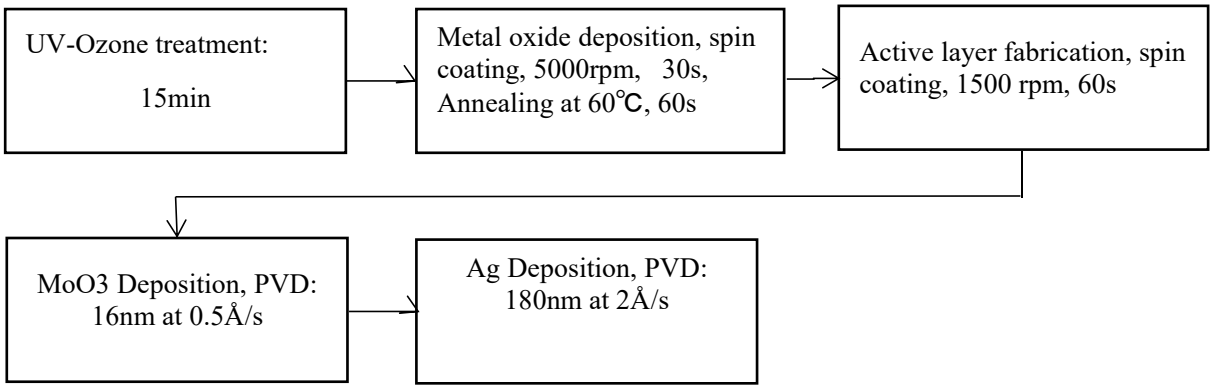

3.4 Film and Device Characterization

1. J-V Curve Test

The J-V curve was tested using a computer-controlled Agilent B2912A precision source meter measurement unit. A solar simulator (Japan Sanyo Co., Ltd., Class AAA, 70×70 cm^2) plus an AM1.5G solar spectrum filter was used as the light source, and the optical power was 100 milliwatts per square centimeter. Polycrystalline silicon (SRC-1000-TC-QZ) is the standard battery. Unless otherwise specified, the area of the device prepared in this paper is 1 mm^2 and the average data is calculated from at least 20 independent devices. The J-V test is the most basic test for organic solar cells. The result is that the energy conversion efficiency is the most basic and important indicator of organic solar cells.

2. External Quantum Efficiency (EQE)

The EQE spectrum was tested with the solar cell spectral response measurement system QE-R3011 (Taiwan Gwangyang Co., Ltd.). The light intensity at each wavelength is corrected by a standard polysilicon solar cell. Not only can the EQE spectrum study the electrical response of organic solar cells at different wavelengths of incident light, but their integrated current density can also be used as a verification value for J-V testing.

3. Grained Incident Wide-angle X- ray Scattering

Grained incident wide-angle X-ray scattering was also tested at the Center for Advanced Light Sources in Berkeley, USA, with a beamline of 7.3.3 and an incident angle of 0.14 degrees. The detected X-rays were counted using a Dectris Pilatus 2M photodetector. The solid film sample was prepared on a silicon substrate. The penetrating wide-angle X-ray scattering can characterize the crystallization state and molecular packing of the active layer film, and it can be detected in

two dimensions. It is the most effective thin film characterization method at present. In addition, the grazing incidence method can detect the depth of several tens of nanometers on the surface of the thin film and can completely eliminate the interference from the substrate.

4. X-ray Diffraction

X-ray diffraction was tested on a Rigaku D/max-2500 X-ray diffractometer using a reflection mode. It uses 2 KW Cu-Ka ray data acquisition at 40 KV and 200 mA. The solid film uses a silicon wafer as a substrate and is calibrated with a blank silicon wafer before testing. X-ray diffraction can be used to characterize samples with more crystallized and thicker thicknesses. However, because of the thinness of the active layer in organic solar cells and the generally weaker crystals, this test is currently being used less and less.

4. Results and Discussion

4.1 Device Structure

An inverted device structure is employed in this study. The schematic structure of Organic Photovoltaic device is shown in Fig. 4.1, using silver as the anode, donor/acceptor bulk heterojunction as active layer, ITO as the cathode.

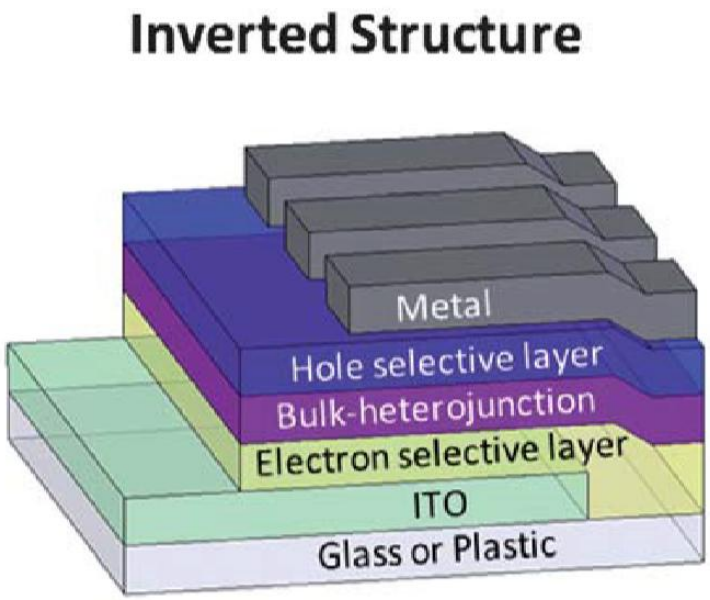

Figure 4.1 Basic device structure of OPV

4.2 Polymer Donor Side Chain Dependency of OPV Device Performance

Previous studies reported the synthesis of seven PTB polymers with the same alternating thienothiophene (**TT**) and benzodithiophene (**BDT**) backbone sequence but with varied side chains; their corresponding solar cell PCEs range from 2-8%. The structural differences among these seven polymers arise from the aliphatic side chains appended at different backbone positions, as shown in Figure 3.1. In the first **PTB** polymer of this series, PTB1, a remarkable

“face-on” polymer backbone orientation in which the π-conjugated polymer backbone planes lie parallel to the substrate surface, resulting in maximal contacts between organic photo-active materials and the ITO anode coated with electron transport layer (ZnO). This orientation of the π-π stacked structures would favor charge transport across the interface. In contrast, most other bulk-heterojunction (BHJ)-OPV materials, such as (P3HT), have a strong preference for an “edge-on” orientation, in which the π-conjugated polymer backbone planes lie nearly perpendicular to the anode surface. Based on this knowledge, the reason why BDTP-Bz-2 shows better device performance than BDTP-Bz-1 can be attributed to its preference for the “face-on” polymer backbone orientation, which would favour the charge transport between the active layer and the electrode.

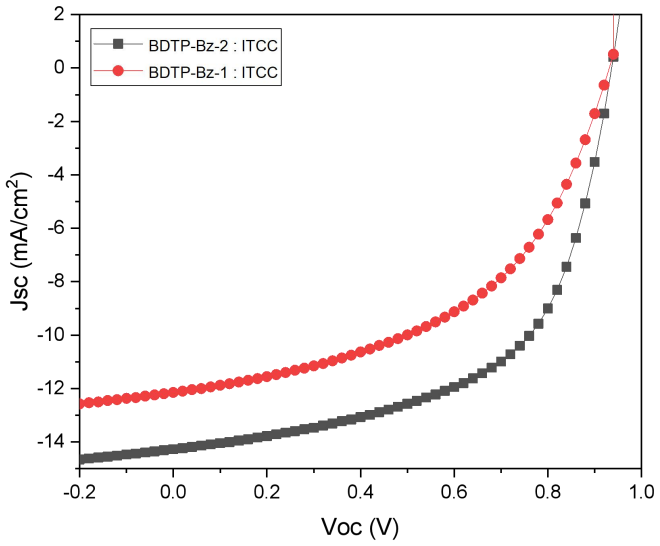

Figure 4.2 Current-voltage (J-V) curve of BDTP-Bz-1 and BDTP-Bz-2

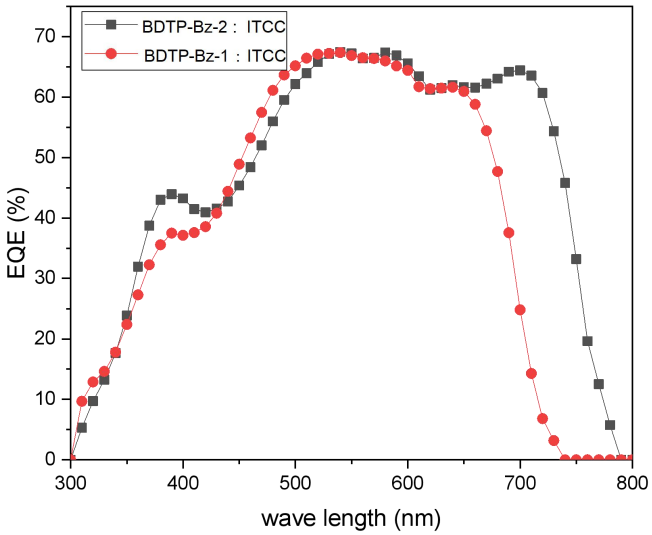

Figure 4.3 External Quantum Efficiency (EQE) of BDTP-Bz-1 and BDTP-Bz-2

Table 4.1 Electrical properties of OPV with BDTP-Bz-1 : ITCC and BDTP-Bz-2 : ITCC as activce layers

Materials	J_{SC}	V_{OC}	Efficiency	FF
BDTP-Bz-1 : ITCC	13.11	0.908	6.00	50.31
BDTP-Bz-2 : ITCC	14.27	0.945	7.72	58.75

4.3 Surface Morphology of BDTP-Bz-1 and BDTP-Bz-2

In order to the understand the side chain effect on the morphology and microstructure of the active layer of OPV, AFM surface topography of BDTP-Bz-1 and BDTP-Bz-2 active layer was measured, shown in Fig. 4.4. It is obvious that both AFM images of BDTP-Bz-1 : ITCC and BDTP-Bz-2 : ITCC active layer film show good uniformity in AFM image without any large feature. As the BDTP-Bz-1 : ITCC and BDTP-Bz-2 : ITCC active layers were fabricated on the

electron transport layer ZnO thin film, and the R_{rms} of the ZnO thin film on ITO substrate (annealing temperature 60℃,1 min) is relatively stable, which is 2.6 nm, so the variation of the surface morphology of BDTP-Bz-1 : ITCC and BDTP-Bz-2 : ITCC can be attribute to the different side chain arrangement. The BDTP-Bz-1 : ITCC has a roughness R_{max} of 12.5 nm and R_{rms} 1.53 nm, BDTP-Bz-2 : ITCC shows improved roughness R_{max} of 10.6 nm and R_{rms} 1.26 nm. R_{max} stands for the peak height of surface roughness and R_{rms} stands for root mean square roughness, which is the mean value from eight different locations on the sample. For a smoother surface, it tends to form a better contact between the active layer and the hole transport layer MnO_3 during the thermal evaporation process. These results indicate that BDTP-Bz-2 : ITCC active layer forms better interface contact with the electrode than BDTP-Bz-1, due to its "face-on" orientation preference of the conjugated backbone, and therefore it is beneficial to the charge transport process.

(a) (b)

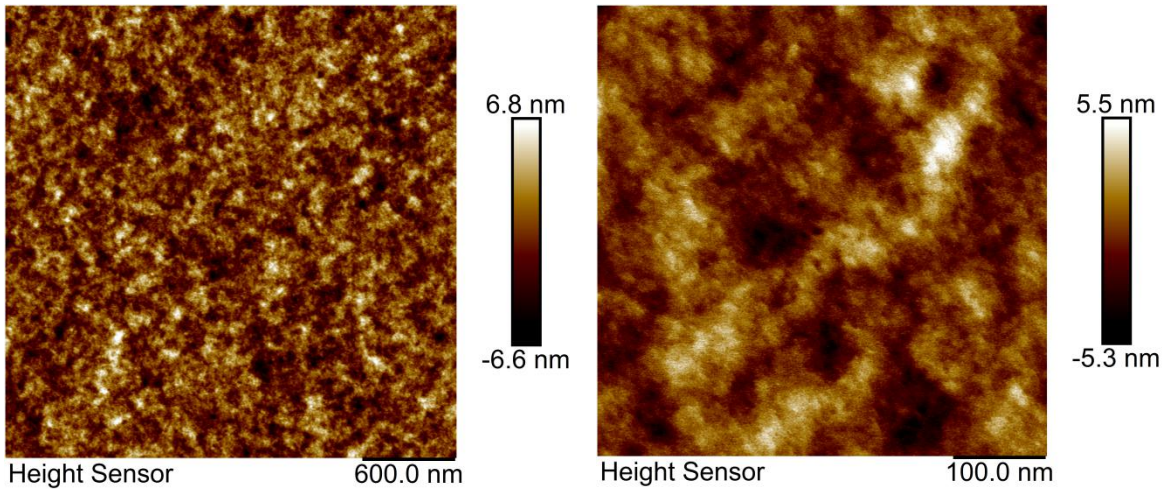

(c)

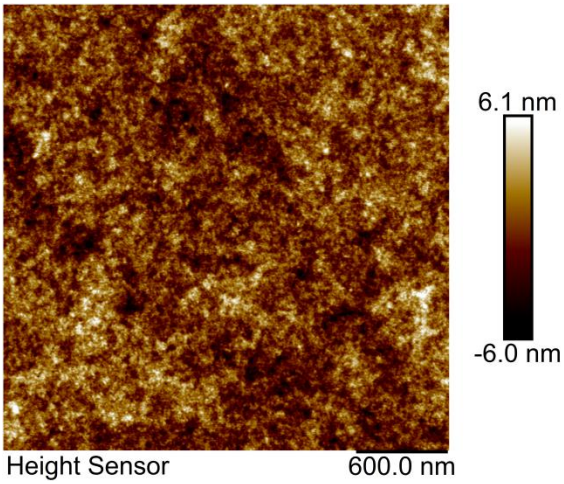

(d)

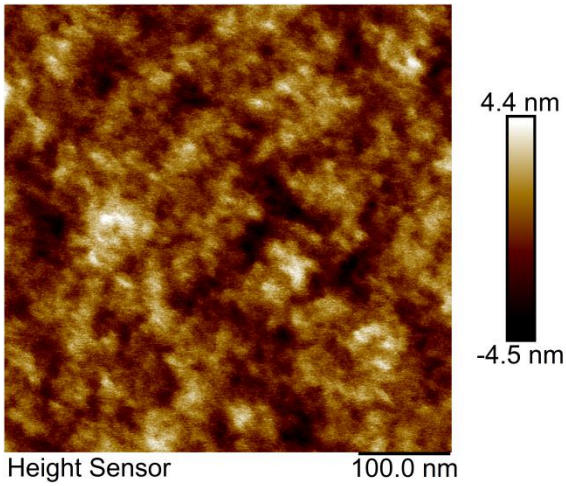

(e)

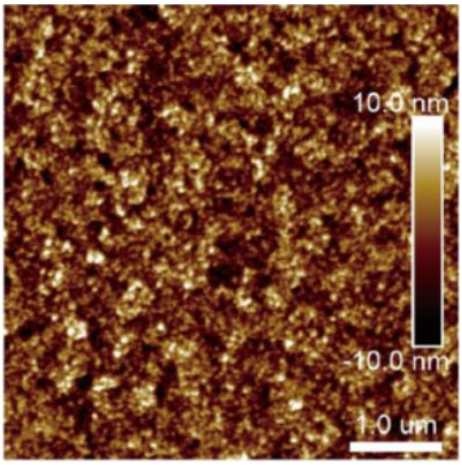

Figure 4.4 (a), (b) AFM image of BDTP-Bz-1 active layer; (c), (d) AFM image of BDTP-Bz-2 active layer

(e) AFM image of ZnO electron transport layer

The X-ray scattering technique is also used to further probe the crystallization behavior of BDTP-Bz-1 : ITCC or BDTP-Bz-2 : ITCC active layer， the results indicate that: 1) branched long alkyl side chain attached at the benzene unit on BDTP-Bz-1cause an increase in the π-π stacking spacing in films and a decrease in the OPV device PCE; 2) there is a positive correlation

between the strength of π-π interactions through the polymer backbone staking in the film and the OPV device fill factor, which is attributed to BDTP-Bz-1 and BDTP-Bz-2 interactions with the anode interfacial layer; 3) the film fabrication with an additive 1,8 diiodooctane (DIO) slightly enhances the crystallinity of the polymers. From these results, we propose that the structure of the donor BDTP-Bz-1 and BDTP-Bz-2 polymer both inhibits long-range crystallinity and facilitates stronger donor and acceptor interactions in the films, thereby enhancing solar cell performance.

The π-π stacking distance between donor polymers BDTP-Bz-1 and BDTP-Bz-2 can be attributed from the structural differences between the alkyl side chains attached to the benzene unit. Two linear alkyl side chains occupy less space than branched alkyl side chain in the π-π stacking direction. For these two polymers, the FF is the electronic property that has the strongest correlation with the π-π stacking distance, this funding has implications for the nature of both the film morphology and the interaction between these donor polymers and underlying ZnO anode interfacial layer. The polymer with the strongest π-π stacking have the most crystalline polymer domains and bind most strongly to the anode interfacial layer. Previous studies have shown that BHJ device FFs can be substantially enhanced by interfacial layers that enhance hole extraction and block undesired electron leakage.

4.4 Proposed Mechanism

The π-π stacking distance between donor polymers BDTP-Bz-1 and BDTP-Bz-2 can be attributed from the structural differences between the alkyl side chains attached to the benzene unit. Two linear alkyl side chains occupy less space than branched alkyl side chain in the π-π

stacking direction. For these two polymers, the FF is the electronic property that has the strongest correlation with the π-π stacking distance, this finding has implications for the nature of both the film morphology and the interaction between these donor polymers and underlying ZnO anode interfacial layer. The polymer with the strongest π-π stacking have the most crystalline polymer domains and bind most strongly to the anode interfacial layer. Previous studies have shown that BHJ device FFs can be substantially enhanced by interfacial layers that enhance hole extraction and block undesired electron leakage.

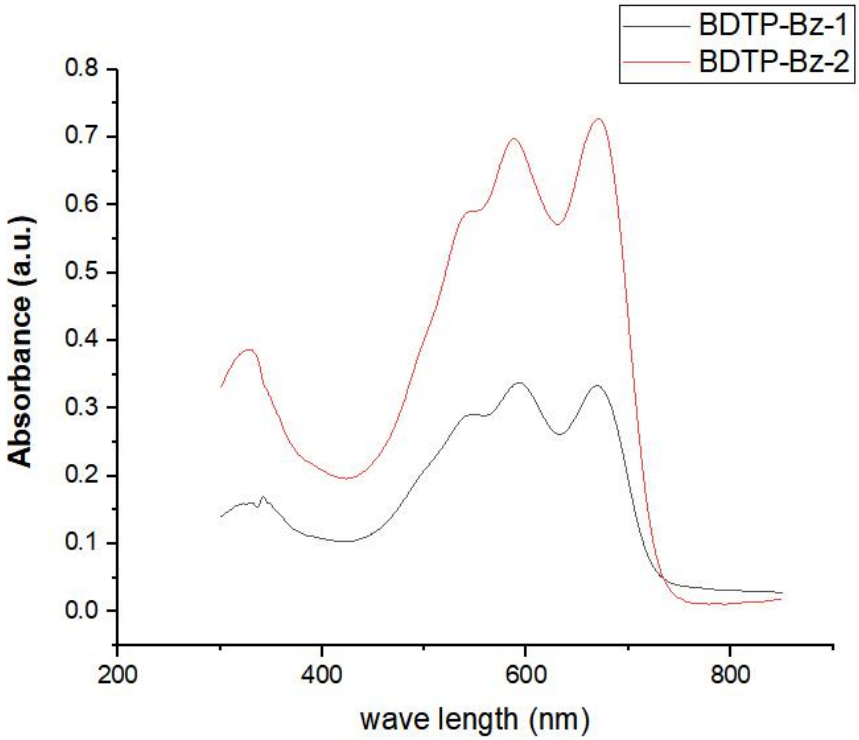

Figure 4.5: Absorbance of film formed by BDTP-Bz-1 and BDTP-Bz-2

Fig. 4.5 compares the absorbance of thin film formed by BDTP-Bz-1 : ITCC and BDTP-Bz-2 : ITCC at wavelength ranges from 300 nm to 800 nm. The BDTP-Bz-2 : ITCC shows better

absorbance at wavelength from 300 nm to around 700 nm while both of BDTP-Bz-2 : ITCC and BDTP-Bz-1 : ITCC show absorption dual peak at around 600 nm and 700 nm respectively.

5. Conclusions

It has been known that the akyl side chains on different positions of the polymer conjugated backbone will lead to various device performance. Typically, the "face-on" polymer backbone orientation in which the π-conjugated polymer backbone planes lie parallel to the substrate surface will result in maximal contacts between the organic photo-active materials and the ITO anode coated with a ZnO interfacial laer. This can partially explain why the PCE and J_{sc} of BDTP-Bz-2 improved 30% and 9% respectively comparing with BDTP-Bz-1, as its orientation of the π-π stacked structures would favor charge transport across the interface.

In conclusion, the film morphology is very sensitive to the structure of the BDTP-Bz-1 and BDTP-Bz-2 side groups attached to the benzene subunits. Differences in how the structure depends on the subunit side groups are attributed to the π-π stacking interactions. BDTP-Bz-2 has stronger stronger π-π stacking due to its two short straight side chains make the space between the conjugated π-π planes smaller than BDTP-Bz-1, whose long branched side chains make the plane-interval large.

6. Scope of Future Work

The starting point of this study is to understand how the position of polymer donor sidechains affect the performance of the organic photovoltaics. The study focus on the side chains on benzene subunit. More research should be done to study how the side chains on other subunits such as alternating thienothiophene (TT) and benzodithiophene (BDT) backbone sequence affect the microstructure and the morphology of the active layer and therefore the overall performance of OPV.

There is an absorbance dual-peak around 600 nm - 700 nm for both BDTP-Bz-1 : ITCC and BDTP-Bz-2 : ITCC and the reason for this phenomena remains unclear. And more work should be done to study how the position of sidechains on polymer donors affect the absorption peak.

As we already know that the side chain position of polymer donor has a strong effect of the orientation of π-π conjugated planes and therefore the BHJ morphology/microstructure, subtle changes in the electronic and side-chain structures in this framework should lead to a large, informative data set for optimizing structure and OPV efficiency.

7. References

1. Cheng and X. Zhan, Stability of organic solar cells: challenges and strategies, Chem. Soc. Rev., 2016, 45, 2544-2582.

2. C. J. Brabec, M. Heeney, I. McCulloch and J. Nelson, Influence of blend microstructure on bulk heterojunction organic photovoltaic performance, Chem. Soc. Rev., 2011, 40, 1185-1199.

3. L. Lu, T. Zheng, Q. Wu, A. M. Schneider, D. Zhao and L. Yu, Recent advances in bulk heterojunction polymer solar cells, Chem. Rev., 2015, 115, 12666-12731.

4. D. M. Chapin, C. S. Fuller and G. L. Pearson, A new silicon p-n junction photocell for converting solar radiation into electrical power, J. Appl. Phys., 1954, 25, 676-677.

5. C. W. Tang, Two-layer organic photovoltaic cell, Appl. Phys. Lett., 1986, 48, 183-185.

6. N. S. Sariciftci, L. Smilowitz, A. J. Heeger and F. Wudl, Photoinduced electron-transfer from a conducting polymer to buckminsterfullerene, Science, 1992, 258, 1474-1476.

7. G. Yu, J. Gao, J. C. Hummelen, F. Wudl and A. J. Heeger, Polymer photovoltaic cells - enhanced efficiencies via a network of internal donor-acceptor heterojunctions, Science, 1995, 270, 1789-1791.

8. J. Zhao, Y. Li, G. Yang, K. Jiang, H. Lin, H. Ade, W. Ma and H. Yan, Efficient organic solar cells processed from hydrocarbon solvents, Nat. Energy, 2016, 1, 15027.

9. Y.-J. Cheng, S.-H. Yang and C.-S. Hsu, Synthesis of Conjugated polymers for organic solar cell applications, Chem. Rev., 2009, 109, 5868-5923.

10. H. A. M. van Mullekom, J. A. J. M. Vekemans, E. E. Havinga and E. W. Meijer, Developments in the chemistry and band gap engineering of donor–acceptor substituted conjugated polymers, Mater. Sci. Eng. R-Rep., 2001, 32, 1-40.

11. J. J. M. Halls, K. Pichler, R. H. Friend, S. C. Moratti and A. B. Holmes, Exciton diffusion and dissociation in a poly(p-phenylenevinylene)/C60 heterojunction photovoltaic cell, Appl. Phys. Lett., 1996, 68, 3120-3122.

12. V. I. Arkhipov, P. Heremans and H. Bässler, Why is exciton dissociation so efficient at the interface between a conjugated polymer and an electron acceptor?, Appl. Phys. Lett., 2003, 82, 4605-4607.

13. P. W. M. Blom, V. D. Mihailetchi, L. J. A. Koster and D. E. Markov, Device physics of polymer : fullerene bulk heterojunction solar cells, Adv. Mater., 2007, 19, 1551-1566.

14. A. C. Arias, J. D. MacKenzie, R. Stevenson, J. J. M. Halls, M. Inbasekaran, E. P. Woo, D. Richards and R. H. Friend, Photovoltaic performance and morphology of polyfluorene blends: a combined microscopic and photovoltaic investigation, Macromolecules, 2001, 34, 6005-6013.

15. O. Inganäs, L. S. Roman, F. Zhang, D. M. Johansson, M. R. Andersson and J. C. Hummelen, Recent progress in thin film organic photodiodes, Synth. Met., 2001, 121, 1525-1528.

16. Y. F. Li, Molecular design of photovoltaic materials for polymer solar cells: toward suitable electronic energy levels and broad absorption, Acc. Chem. Res., 2012, 45, 723-733.

17. G. A. Chamberlain, Organic solar cells: A review, Solar Cells, 1983, 8, 47-83.

18. G. Yu, C. Zhang and A. J. Heeger, Dual-function semiconducting polymer devices: Light-emitting and photodetecting diodes, Appl. Phys. Lett., 1994, 64, 1540-1542.

19. N. S. Sariciftci, L. Smilowitz, A. J. Heeger and F. Wudl, Semiconducting polymers (as donors) and buckminsterfullerene (as acceptor): photoinduced electron transfer and heterojunction devices, Synth. Met., 1993, 59, 333-352.

20. R. Meerheim, C. Körner and K. Leo, Highly efficient organic multi-junction solar cells with a thiophene based donor material, Appl. Phys. Lett., 2014, 105, 063306.

21. L. Zuo, C.-C. Chueh, Y.-X. Xu, K.-S. Chen, Y. Zang, C.-Z. Li, H. Chen and A. K. Y. Jen, Microcavity-enhanced light-trapping for highly efficient organic parallel tandem solar cells, Adv. Mater., 2014, 26, 6778-6784.

22. C.-C. Chen, W.-H. Chang, K. Yoshimura, K. Ohya, J. You, J. Gao, Z. Hong and Y. Yang, An efficient triple-junction polymer solar cell having a power conversion efficiency exceeding 11%, Adv. Mater., 2014, 26, 5670-5677.

23. A. R. b. M. Yusoff, D. Kim, H. P. Kim, F. K. Shneider, W. J. da Silva and J. Jang, A high efficiency solution processed polymer inverted triple-junction solar cell exhibiting a power conversion efficiency of 11.83%, Energy Environ. Sci., 2015, 8, 303-316.

24. M. T. Dang, L. Hirsch and G. Wantz, P3HT:PCBM, Best seller in polymer photovoltaic research, Adv. Mater., 2011, 23, 3597-3602.

25. L. Ye, S. Zhang, L. Huo, M. Zhang and J. Hou, Molecular design toward highly efficient photovoltaic polymers based on two-dimensional conjugated benzodithiophene, Acc. Chem. Res., 2014, 47, 1595-1603.

26. J. Chen and Y. Cao, Development of novel conjugated donor polymers for high-efficiency bulk-heterojunction photovoltaic devices, Acc. Chem. Res., 2009, 42, 1709-1718.

27. J.-S. Wu, S.-W. Cheng, Y.-J. Cheng and C.-S. Hsu, Donor-acceptor conjugated polymers based on multifused ladder-type arenes for organic solar cells, Chem. Soc. Rev., 2015, 44, 1113-1154.

28. C. Liu, K. Wang, X. Gong and A. J. Heeger, Low bandgap semiconducting polymers for polymeric photovoltaics, Chem. Soc. Rev., 2016, DOI: 10.1039/C5CS00650C.

29. S. Guenes, H. Neugebauer and N. S. Sariciftci, Conjugated polymer-based organic solar cells, Chem. Rev., 2007, 107, 1324-1338.

30. L. Dou, Y. Liu, Z. Hong, G. Li and Y. Yang, Low-bandgap near-ir conjugated polymers/molecules for organic electronics, Chem. Rev., 2015, 115, 12633-12665.

31. H.-Y. Chen, J. Hou, S. Zhang, Y. Liang, G. Yang, Y. Yang, L. Yu, Y. Wu and G. Li, Polymer solar cells with enhanced open-circuit voltage and efficiency, Nat. Photon., 2009, 3, 649-653.

32. Y. Liang, Z. Xu, J. Xia, S.-T. Tsai, Y. Wu, G. Li, C. Ray and L. Yu, For the bright future—bulk heterojunction polymer solar cells with power conversion efficiency of 7.4%, Adv. Mater., 2010, 22, E135-E138.

33. L. J. Huo, S. Q. Zhang, X. Guo, F. Xu, Y. F. Li and J. H. Hou, Replacing alkoxy groups with alkylthienyl groups: a feasible approach to improve the properties of photovoltaic polymers, Angew. Chem.-Int. Edit., 2011, 50, 9697-9702.

34. S.-H. Liao, H.-J. Jhuo, Y.-S. Cheng and S.-A. Chen, Fullerene derivative-doped zinc oxide nanofilm as the cathode of inverted polymer solar cells with low-bandgap polymer (PTB7-Th) for high performance, Adv. Mater., 2013, 25, 4766-4771.

35. Y. Lin, Y. Li and X. Zhan, Small molecule semiconductors for high-efficiency organic photovoltaics, Chem. Soc. Rev., 2012, 41, 4245-4272.

36. Y. Chen, X. Wan and G. Long, High performance photovoltaic applications using solution-processed small molecules, Acc. Chem. Res., 2013, 46, 2645-2655.

37. J. Roncali, Molecular Bulk heterojunctions: an emerging approach to organic solar cells, Acc. Chem. Res., 2009, 42, 1719-1730.

38. T. S. van der Poll, J. A. Love, T. Q. Nguyen and G. C. Bazan, Non-basic high-performance molecules for solution-processed organic solar cells, Adv. Mater., 2012, 24, 3646-3649.

39. J. Zhou, X. Wan, Y. Liu, Y. Zuo, Z. Li, G. He, G. Long, W. Ni, C. Li, X.-C. Su and Y. Chen, Small molecules based on benzo[1,2-b:4,5-b']dithiophene unit for high-performance solution processed organic solar cells, J. Am.Chem. Soc., 2012, 134, 16345-16351.

40. B. Kan, Q. Zhang, M. Li, X. Wan, W. Ni, G. Long, Y. Wang, X. Yang, H. Feng and Y. Chen, Solution-processed organic solar cells based on dialkylthiol-substituted benzodithiophene unit with efficiency near 10%, J. Am. Chem. Soc., 2014, 136, 15529-15532.